Deep-Water Acoustic Coherence at Long Ranges: Theoretical Prediction and Effects on Large-Array Signal Processing

Elena Yu. Gorodetskaya, Alexander I. Malekhanov, Alexander G. Sazontov, and Nadezhda K. Vdovicheva

***Abstract*— This paper presents results of combined consideration of sound coherence and array signal processing in long-range deep-water environments. Theoretical evaluation of the acoustic signal mutual coherence function (MCF) of space for a given sound-speed profile and particular scattering mechanism is provided. The predictions of the MCF are employed as input data to investigate the coherence-induced effects on the horizontal and vertical array gains associated with linear and quadratic beamformers with emphasis on the optimal ones. A method of the radiation transport equation is developed to calculate the MCF of the multimode signal under the assumption that internal waves or surface wind waves are the main source of long-range acoustic fluctuations in a deep-water channel. Basic formulations of the array weight vectors and small-signal deflection are then exploited to examine optimal linear and quadratic processors in comparison with plane-wave beamformers. For vertical arrays, particular attention is paid also to evaluation of the ambient modal noise factor. The numerical simulations are carried out for range-independent environments from the Northwest Pacific for a sound frequency of 250 Hz and distances up to 1000 km. It was shown distinctly that both signal coherence degradation and modal noise affect large-array gain, and these effects are substantially dependent on the processing technique used. Rough surface sound scattering was determined to cause the most significant effects.**

***Index Terms*— Array beamforming, long-range propagation, mutual coherence function, radiation transport equation, random scattering.**

I. Introduction

LONG-RANGE acoustic signal propagation in underwater channels is known to lead to loss of the signal coherence in space, time, and frequency, which results from multiple sound scattering by random inhomogeneities of the oceanic medium (see, e.g., [1], [2]). From an application point of view, the knowledge of the spatial-temporal mutual coherence function (MCF) of the registered acoustic field is of the utmost importance to optimize signal processing techniques and, therefore, to decrease a coherence-induced degradation of the processor performances.

Manuscript received July 1, 1998; revised December 15, 1998. This work was supported by the Russian Foundation for Basic Research under Grant 96-02-19444a and by the TNO Electronics and Physics Laboratory (The Netherlands) under Contract 95/857.

E. Gorodetskaya, A. Malekhanov, and A. Sazontov are with the Division of Hydrophysics and Hydroacoustics, Institute of Applied Physics, Russian Academy of Science, Nizhny Novgorod, Russia.

N. Vdovicheva is with the Institute for Physics of Microstructures, Russian Academy of Science, Nizhny Novgorod, Russia.

Publisher Item Identifier S 0364-9059(99)03034-4.

Following the general idea of spatial-temporal processing factorization, we restrict ourselves to the study of coherence effects in the spatial domain, which is of primary interest in large-array beamforming. The problem of array processing under the conditions of reduced signal coherence was studied earlier by several authors [3]–[6] on the basis of a general theory of random signal detection against the noise background [7], [8], but without invoking specific models for underwater sound coherence. On the other hand, the subjects of numerous works on ocean acoustic coherence were restricted, as a rule, to the propagation problem itself.

In this paper, we present our recent results on combined consideration of the sound wavefield coherence and array signal processing in long-range deep-water environments. A distinctive feature of our study is incorporating detailed calculations of the total signal MCF of space [9]–[11] to predict the coherence effects on the array beam pattern and gain for several types of linear and quadratic processors, including the optimal ones [12]–[14].

The scheme of our study is outlined as follows. For calculations of the ocean acoustic MCF, we develop a technique of the radiation transport equation (RTE) and derive in a closed form a useful approximate solution for the multimodal MCF. In our comparative analysis of array processors, we exploit, as a basic approach, the eigenvalue–eigenvector decomposition of the signal covariance matrices. Generally, this approach can be effectively used for various detection criteria, including maximum likelihood (ML) and maximum signal-to-noise (SNR). Our particular interest here concerns the small-signal asymptotics of the ML detection performance, which is a reasonable choice for long-range underwater acoustics.

The body of this paper follows the scheme summarized above. The wave-theoretical model of acoustic transmission in a random-inhomogeneous oceanic waveguide is reviewed in Section II, which contains a brief discussion of the RTE technique that has been developed to calculate the ocean acoustic MCF for long-range multimode propagation. We present in Section III the most significant aspects of large-array processing of partially coherent signals with an emphasis on comparative analysis of linear and quadratic beamformers, including the optimal ones. Next, in Section IV, we address the results of the numerical simulations of long-range acoustic signal propagation and array processing using seasonally averaged profiles from the Northwest Pacific. Calculations of the expected acoustic coherence in special cases of internal-wave

medium fluctuations and fully developed wind seas are employed to show in detail the acoustic coherence effects on the array beampattern and gain for several types of beamformers, including both horizontal and vertical array configurations. Finally, in Section V, we summarize the results obtained and give the most essential conclusions from this study.

II. Ocean Acoustic Coherence: Wave-Theoretical Description

The acoustic propagation problem in a random ocean is of great interest for various applications concerned with underwater detection, communication, and ocean acoustic tomography. The significant and unusual characteristics of the ocean medium are the presence of an underwater sound channel and the anisotropy and inhomogeneity of the sound-speed fluctuations. Thus, the study of the combined effects of anisotropic scattering and regular refraction on acoustic coherence is of great importance in understanding statistical behavior of oceanic sound transmission. From the theoretical point of view, analysis of this problem reduces to evaluating the MCF of space, time, and frequency. The MCF contains important statistical properties of the acoustic field that has traversed a medium with random fluctuations.

A. Preliminaries

Systematic investigations examining the propagation of the MCF in a refractive oceanic waveguide containing random inhomogeneities have recently been carried out in the framework of a ray-oriented approach using the path integral formalism. The predictions of acoustic coherence from the path integral theory and its comparisons with single-receiver measurements are fairly well summarized in the book by Flatte *et al.* [1]. It should be noted that a solution for the MCF equivalent to that obtained by path integral methods can be derived as the first approximation of the second moment equation when only one path of multipath configuration is treated [15], [16].

For low-frequency long-range multipath propagation, there is an effective alternative approach based upon the normal-mode method. The use of this treatment introduces the effect of the sound-speed profile in a direct and systematic way. Applied to ocean acoustics, the modal approach has been developed in a series of publications (see, e.g., [17]–[32]. The statistical description of stochastic waveguide propagation usually deals with a set of differential equations for the self-modal and cross-modal coherence functions that predict the evolution in range for both the energy and correlation characteristics of an underwater acoustic field. These equations can be solved at least with the aid of a computer. For a low-frequency regime, a general computer program has been developed by Dozier and Tappert [21] and Beilis and Tappert [22] to evaluate the effects of volume and rough surface scattering on transmission loss as a function of range and depth in a canonical-model random ocean. However, when a large number of propagating modes is present, the numerical integration becomes rather cumbersome and, hence, there is a need to develop approximate analytical methods.

Most of the research using the normal-mode decomposition has been restricted primarily to the average wavefield intensity evolution that was obtained by means of a diffusion approach [17], [20], [27], [28] when a discrete set of guided modes is regarded as a continuum. The analytical works concerning the correlation characteristics of a multimode signal have also been tried by the use of a matrix analog of the Rytov approximation, although their results are applicable only to cases of relatively short propagation distances [26], [30], [32].

Considerable progress in the theoretical study of acoustic coherence for a large class of scattering models in long-range ocean environments has been recently achieved by Sazontov [9], [10], who proposed an efficient method for solving the RTE for multimodal propagation. Below, we present a useful approximate wave-theoretical expression for the total MCF which is valid for a wide range of refractive index profiles and types of scattering irregularities. It is important to have such a solution since it enables one to study the acoustic propagation and loss of coherence in deep-water environments.

B. Volume Scattering: Problem Formulation

Consider an underwater sound channel of depth H, in which the refractive index is the sum of the deterministic background profile $n_0(z)$ depending on vertical coordinate z and of the stochastic field $\mu(\mathbf{r}, z, t)$ modeling the acoustic medium fluctuations. Here, $\mathbf{r} = (x, y)$ is the horizontal two-dimensional (2-D) position vector and t is the time. The coordinate system is chosen with the z axis downwards. The perturbation μ is assumed to be a Gaussian random variable with zero mean and can be described by its autocorrelation function

$$\langle \mu(\mathbf{r}_1, z_1, t_1)\mu(\mathbf{r}_2, z_2, t_2)\rangle = B_\mu(|\mathbf{r}_1 - \mathbf{r}_2|, z_1, z_2, t_1 - t_2).$$

The angular brackets $\langle\cdots\rangle$ indicate ensemble averaging.

Let a nondirectional acoustic source be located at coordinates $(0, z_0)$ and emit a signal having time dependence $g(t) = s(t)\exp(-i\omega_0 t)$, where $\omega_0 = 2\pi f_0$ denotes the radian carrier frequency. In terms of normal modes, the complex envelope of the acoustic pressure field $P(\mathbf{r}, z, t)$ in an irregular oceanic channel far enough from a source can be formally represented by

$$P(\mathbf{r}, z, t) = \int_{-\infty}^{\infty} d\omega\, g(\omega) e^{-i\omega t} \sum_{n=1}^{M(\omega)} P_n(\mathbf{r}, \omega, t)\varphi_n(z, \omega) \tag{1}$$

where $g(\omega)$ is the frequency spectrum of the transmitted signal, $\varphi_n(z, \omega)$ denotes the nth vertical eigenfunction of the deterministic background medium associated with the eigenvalue $\kappa_n^2(\omega)$, M is the number of propagating modes, and $P_n(\mathbf{r}, \omega, t)$ are the random normal mode amplitudes. In writing (1), we ignored the far-field contribution from the modes of continuous spectrum. The normal mode functions $\varphi_n(z, \omega)$ satisfy the eigenvalue problem

$$\frac{d^2}{dz^2}\varphi_n(z, \omega) + \left[k^2 n_0^2(z) - \kappa_n^2(\omega)\right]\varphi_n(z, \omega) = 0 \tag{2}$$

together with appropriate boundary conditions and an orthonormality relation, i.e., $\int_0^H dz\,\varphi_n(z,\omega)\varphi_m(z,\omega) = \delta_{nm}$. Here, $k = \omega/c_0$, where c_0 is some reference sound speed.

In a waveguide with large-scale (compared to the wavelength) inhomogeneities, where the forward scattering is assumed to be essential, we shall use the spatial coordinate system with the x axis taken in the main direction of wave propagation. For forward propagation, if we let

$$P_n(\mathbf{r},\omega,t) = \frac{1}{\sqrt{\kappa_n(\omega)}} p_n(\mathbf{r},\omega,t) e^{i\kappa_n(\omega)x}$$

one obtains from the original wave equation the parabolic coupled-mode equations for the slowly varying coefficients $p_n(\mathbf{r},\omega,t)$

$$\left(\frac{\partial}{\partial x} - \frac{i}{2\kappa_n(\omega)}\frac{\partial^2}{\partial y^2}\right) p_n(\mathbf{r},\omega,t) = i\sum_m V_{nm}(\mathbf{r},\omega,t) p_m(\mathbf{r},\omega,t) \tag{3}$$

where $V_{nm}(\mathbf{r},t)$ is the matrix coupling coefficient (depending on t as a parameter) defined according to

$$V_{nm}(\mathbf{r},\omega,t) = \frac{k^2}{\sqrt{\kappa_n(\omega)\kappa_m(\omega)}} \mu_{nm}(\mathbf{r},\omega,t) e^{-i\kappa_{nm}^-(\omega)x}$$

where

$$\kappa_{nm}^-(\omega) = \kappa_n(\omega) - \kappa_m(\omega)$$
$$\mu_{nm}(\mathbf{r},\omega,t) = \int_0^H dz\, n_0(z)\mu(\mathbf{r},z,t)\varphi_n(z,\omega)\varphi_m(z,\omega). \tag{4}$$

Note that the parabolic approximation consists of considering solutions in which waves are traveling only at small angles to a particular direction. This direction, labeled here by x, is in the horizontal.

The important correlation properties of an acoustic wave that has traversed a random oceanic waveguide are described by the second moment of the pressure field by

$$B_p(\mathbf{r_1}, z_1, t_1 \mid \mathbf{r_2}, z_2, t_2) = \langle P(\mathbf{r_1}, z_1, t_1) P^*(\mathbf{r_2}, z_2, t_2)\rangle \tag{5}$$

where the asterisk denotes the complex conjugate. Inserting the field expansion from (1) into (5), one finds that

$$B_p(\mathbf{r_1}, z_1, t_1 \mid \mathbf{r_2}, z_2, t_2) = \int_{-\infty}^{\infty} d\omega_1 \int_{-\infty}^{\infty} d\omega_2\, g(\omega_1) g^*(\omega_2) \Gamma_s(\cdot \mid \cdot) e^{-i\omega_1 t_1 + i\omega_2 t_2} \tag{6}$$

where $\Gamma_s(\mathbf{r_1}, z_1, \omega_1, t_1 \mid \mathbf{r_2}, z_2, \omega_2, t_2)$ is the total signal MCF defined as

$$\Gamma_s(\mathbf{r_1}, z_1, \omega_1, t_1 \mid \mathbf{r_2}, z_2, \omega_2, t_2) = \sum_{n,m} \frac{\varphi_n(z_1,\omega_1)\varphi_m(z_2,\omega_2)}{\sqrt{\kappa_n(\omega_1)\kappa_m(\omega_2)}} \Gamma_{nm}(1,2) e^{i\kappa_{nm}^-(\omega)x},$$
$$\Gamma_{nm}(1,2) = \langle p_n(1) p_m^*(2)\rangle. \tag{7}$$

The labels 1 and 2 refer to two different horizontal position points, times, and frequencies. Thus, the evaluation of the total MCF applied to the stochastic waveguide propagation requires knowledge of the cross-modal coherence functions $\Gamma_{nm}(1,2)$.

In [32], the basic RTE for the cross-modal MCF $\Gamma_{nm}(1,2)$ taken at two horizontal position points $\mathbf{r_1} = (x, y_1)$, $\mathbf{r_2} = (x, y_2)$ in the same x plane at two different times and frequencies was derived from (3) under the Markov approximation

$$\left[\frac{\partial}{\partial x} - i\xi_{nm}^+ \frac{\partial^2}{\partial\rho\partial R} - \frac{i}{2}\xi_{nm}^- \left(\frac{\partial^2}{\partial\rho^2} + \frac{1}{4}\frac{\partial^2}{\partial R^2}\right)\right]\Gamma_{nm}(1,2) = -\frac{1}{2}\left[\sum_{n'} A_{nn'}(1,1)\Gamma_{n'm}(1,2) + \sum_{m'} A_{m'm}(2,2)\Gamma_{nm'}(1,2)\right] + \sum_{n',m'} A_{nn'}^{mm'}(1,2)\Gamma_{n'm'}(1,2) \tag{8}$$

with the definitions $\rho = y_1 - y_2$, $R = 0.5(y_1 + y_2)$, $\tau = t_1 - t_2$, $\xi_{nm}^+ = 0.5[\kappa_n^{-1}(\omega_1) + \kappa_m^{-1}(\omega_2)]$, $\xi_{nm}^- = \kappa_n^{-1}(\omega_1) - \kappa_m^{-1}(\omega_2)$, $A_{nn'}(1,1) = \sum_{m'} A_{nm'}^{nm'}(1,1)$, and the coupling matrix $A_{nn'}^{mm'}(1,2)$ given by

$$A_{nn'}^{mm'}(1,2) = \int_{-\infty}^{\infty} d\eta \left\langle V_{nn'}\left(x + \frac{1}{2}\eta, y_1, \omega_1, t_1\right) \times V_{mm'}\left(x - \frac{1}{2}\eta, y_2, \omega_2, t_2\right)\right\rangle.$$

As a consequence of (8), we obtain the conservation relation

$$\frac{d}{dx}\sum_{n=1}^{M}\int_{-\infty}^{\infty} \Gamma_{nn}(x, \rho = 0, R, \tau = 0, \omega, \omega)\, dR = 0.$$

In addition to (8), initial conditions of x must be imposed. These conditions, dictated by the source, may be obtained by a matching procedure to give

$$\Gamma_{nm}(1,2)|_{x=0} = \frac{1}{4}\xi_{nm}^+ \varphi_n(z_0,\omega_1)\varphi_m(z_0,\omega_2)\,\delta(\rho)\,\delta(R). \tag{9}$$

With regard to (8) the following point should be noted. If one is interested in long-range propagation, then only nonoscillatory terms contribute appreciably to the system (8). So, in the limit of large x, (8) reduces to

$$\left[\frac{\partial}{\partial x} - i\xi_{nm}^+ \frac{\partial^2}{\partial\rho\partial R} - \frac{i}{2}\xi_{nm}^- \left(\frac{\partial^2}{\partial\rho^2} + \frac{1}{4}\frac{\partial^2}{\partial R^2}\right)\right]\Gamma_{nm}(1,2) = -\frac{1}{2}[A_{nn}(1,1) + A_{mm}(2,2)]\Gamma_{nm}(1,2) + {\sum_{n',m'}}' A_{nn'}^{mm'}(1,2)\Gamma_{n'm'}(1,2)$$

where $\sum'_{n',m'}$ means the summation over all couples of modes satisfying the synchronism condition

$$\kappa_n - \kappa_m = \kappa_{n'} - \kappa_{m'}. \tag{10}$$

Under these circumstances, the diagonal elements of the matrix $\Gamma_{nm}(1,2)$ decouple from the off-diagonal elements, since at $n = m$ the condition (10) will be justified when $n' = m'$. Note

also that the behavior of the off-diagonal elements Γ_{nm} $(n \neq m)$ depends significantly on the type of oceanic waveguide. In particular, for the waveguides having a quasi-equidistant spectrum of wavenumbers κ_n, (10) can be satisfied for a large number of modes n, m and n', m' such that $n-m=n'-m'$. In the opposite case, when the spectrum κ_n is nonequidistant, only the terms with $n = n'$ and $m = m'$ contribute to the double sum.

C. Asymptotic Expression for the Cross-Modal MCF

The set of coupled integrodifferential equations (8) is hard to solve exactly, and numerical simulations are needed. If M becomes too large, the numerical integration of these equations becomes impractical. However, in the quasi-classical approximation, when the WKB formulas are valid for $\varphi_n(z,\omega)$, it is possible to construct an analytical solution for $\Gamma_{nm}(1,2)$ and to obtain a useful approximate representation for the total MCF [9], [10].

The approach employed uses the well-known properties of the quasi-classical elements V_{nm} [see (4)], according to which the corresponding coupling matrix is a function mainly of difference indices of interacting modes [33], [34]

$$\mu_{nn'}(\mathbf{r},\omega,t) = \frac{2}{\Lambda_n}\int_0^{\Lambda_n/2} dx'\, n_0[z_n(x')]\mu(\mathbf{r}, z_n(x'), t) \times \cos\left(\frac{2\pi}{\Lambda_n}(n-n')x'\right)$$

where Λ_n is the mode cycle distance, $z_n(x)$ is the modal ray trajectory satisfying the equation

$$\frac{d^2 z_n(x)}{dx^2} = \frac{1}{2a_n}\frac{d}{dz}\, n_0^2[z_n(x)], \quad a_n = \frac{\kappa_n(\omega)}{k}$$

with

$$\frac{dz_n(x)}{dx} = \frac{1}{a_n}\sqrt{n_0^2(z)-a_n^2} \equiv \tan\chi_n(x), \qquad n_0[z_n(x)]\cos\chi_n(x) = a_n$$

and $\chi_n(x)$ is the angle made by the modal ray and the horizontal at point x.

As a result, (8) can be regarded as a discrete convolution-type equation. This circumstance together with the generating function technique allow us to reduce (8) to the equation which coincides formally with the equation governing the propagation of the MCF in free space. Then, the solution for the generating function can be found analytically. This has the advantage of offering the possibility of obtaining a solution in a closed form for the cross-modal MCF by the Fourier inversion of the generating function to give

$$\Gamma_{nm}(1,2) = \sum_{\nu,\lambda}\int_0^{2\pi}\int \frac{d\alpha\, d\beta}{(2\pi)^2} e^{-i(n-\nu)\alpha + i(m-\lambda)\beta}\Gamma_{\nu\lambda}^{\alpha\beta}(1,2). \tag{11}$$

Here, $\Gamma_{\nu\lambda}^{\alpha\beta}(1,2)$ is defined according to

$$\Gamma_{\nu\lambda}^{\alpha\beta}(1,2) = \Gamma_{\nu\lambda}^{0}(1,2)\exp\left[-\frac{1}{2}D_{\nu\lambda}^{\alpha\beta}(1,2)\right] \tag{12}$$

where

$$\Gamma_{\nu\lambda}^{0}(1,2) = \frac{\varphi_\nu(z_0,\omega_1)\varphi_\lambda(z_0,\omega_2)}{8\pi x} \times \exp\left[\frac{i\rho R}{\xi_{\nu\lambda}^{+}x} - \frac{i\xi_{\nu\lambda}^{-}}{2\xi_{\nu\lambda}^{+}x}\left(R^2+\frac{1}{4}\rho^2\right)\right]$$

is the solution of the transport equation in the absence of random inhomogeneities for a point source situated at coordinates $(0, z_0)$, and the quantity $D_{\nu\lambda}^{\alpha\beta}$ describing the loss of wavefield coherence has the form

$$D_{\nu\lambda}^{\alpha\beta}(1,2) = \int_0^x dx' \left[d_{\nu\nu}^{\alpha\alpha}(x,1 \mid x',1) + d_{\lambda\lambda}^{\beta\beta}(x,2 \mid x',2) - 2d_{\nu\lambda}^{\alpha\beta}(x,1 \mid x',2)\right] \tag{13}$$

where

$$d_{\nu\lambda}^{\alpha\beta}(x,1 \mid x',2) = 2\pi k_1 k_2 \int_{-\infty}^{\infty} d\Omega \cos(\Omega\tau)\int_{-\infty}^{\infty}\int d\text{æ}_y\, d\text{æ}_z \times \frac{\Phi_\mu\left(\boldsymbol{\text{æ}}_{\nu\lambda}(x'),\Omega,z_{\nu\lambda}^{\alpha\beta}(x')\right)}{\cos\chi_\nu(x')\cos\chi_\lambda(x')}\cos\left(\text{æ}_y\rho\frac{x'}{x}\right) \times \cos\left(\text{æ}_z\varsigma_{\nu\lambda}^{\alpha\beta}(x')\right).$$

In writing (13), the following notation is used: $\Phi_\mu(\boldsymbol{\text{æ}},\Omega,z)$ is the local spectrum of the sound-speed fluctuations taken at $\boldsymbol{\text{æ}} = \boldsymbol{\text{æ}}_{\nu\lambda}^{\alpha\beta}(x)$, where the wavenumber $\boldsymbol{\text{æ}}_{\nu\lambda}^{\alpha\beta}(x)$ has the components

$$\boldsymbol{\text{æ}}_{\nu\lambda}^{\alpha\beta}(x) = \left(-0.5\left(\tan\chi_\nu^\alpha(x)+\tan\chi_\lambda^\beta(x)\right)\text{æ}_z, \text{æ}_y, \text{æ}_z\right)$$

$\tan\chi_\nu^\alpha(x) = dz_\nu^\alpha(x)/dx$ is the inclination of a modal ray with the path $z_\nu^\alpha(x) \equiv z_\nu(x-\alpha\Lambda_\nu/2\pi)$, $z_{\nu\lambda}^{\alpha\beta}(x) = 0.5(z_\nu^\alpha(x) + z_\lambda^\beta(x))$, and $\xi_{\nu\lambda}^{\alpha\beta}(x) = z_\nu^\alpha(x) - z_\lambda^\beta(x)$.

Equation (13) for $D_{\nu\lambda}^{\alpha\beta}(1,2)$ is immediately recognized as the phase-structure function (PSF) with the only difference being that the integral in (13) is taken along a modal ray instead of a usual geometric ray. The combination $d_{\nu\nu}^{\alpha\alpha}(x,1 \mid x',1) + d_{\lambda\lambda}^{\beta\beta}(x,2 \mid x',2) - 2d_{\nu\lambda}^{\alpha\beta}(x,1 \mid x',2)$ can now be regarded as a density of the PSF. Such a ray-modal analogy allows one to use in the calculation of coherence the well-known results for the PSF obtained in the framework of the ray theory.[1]

Equations (6), (7), and (11)–(13) present in a closed form a useful approximate solution to the problem of interest. For a given sound-speed profile and spectrum of the volume medium fluctuations, they give explicit rules for calculating both the correlation function and the wavefield intensity in a random oceanic waveguide. The restrictions on the theory are detailed in [9] and [10].

D. Rough Surface Scattering Effects on the MCF

Equation (3) describes the coupling between the normal mode amplitudes due to random volume irregularities of refractive index. In certain environments, for example, when the propagation takes place in an upper sound channel, surface interactions play a predominant role in acoustic signal fluctuations. The formalism developed in [9] and [10] may be

[1]The methods for evaluating the PSF from a general internal-wave model [35] were presented by Esswein and Flatte [36].

extended to the analysis of acoustic coherence after long-range multiple surface scatterings. This can be done as follows.

In the presence of a soft boundary $z = \eta(\mathbf{r}, t)$, where η represents random displacements of the ocean surface, in addition to the wave equation, the following condition on the acoustic pressure field is imposed:

$$P(\mathbf{r}, \eta(\mathbf{r}, t), t) = 0.$$

Concerning the statistics of $\eta(\mathbf{r}, t)$, we assume that $\eta(\mathbf{r}, t)$ is a Gaussian homogeneous and stationary field with zero mean and is characterized by the spatial-temporal correlation function B_η

$$B_\eta(\rho, \tau) = \langle \eta(\mathbf{r}, t)\eta(\mathbf{r} + \rho, t + \tau)\rangle.$$

For a small Rayleigh parameter, the explicit boundary condition can be expanded at the mean ocean surface $z = 0$ in powers of η to give

$$P(\mathbf{r}, 0, t) = -\eta(\mathbf{r}, t)\frac{\partial P(\mathbf{r}, z, t)}{\partial z}\bigg|_{z=0}.$$

In the case considered, it is straightforward to show that the normal mode amplitudes $p_n(\mathbf{r}, t)$ in (1) formally obey the set of stochastic equations (3) in which the coupling coefficients V_{nm} are now defined according to [17]

$$V_{nm}(\mathbf{r}, \omega, t) = \frac{\varphi_n'(0, \omega)\varphi_m'(0, \omega)}{2\sqrt{\kappa_n(\omega)\kappa_m(\omega)}}\eta(\mathbf{r}, t)e^{-i\kappa_{nm}^{-}(\omega)x}$$

where the prime denotes differentiation with respect to depth z.

Hence, rough surface and volume scattering effects can be formally described in the framework of a united approach, and the particular scattering mechanism specifies the concrete form of the coupling elements V_{nm}. Therefore, the equations governing the propagation of the MCF in a waveguide with a rough surface are the same as before except that the coupling matrix $A_{nn'}^{mm'}(1, 2)$ must be replaced by

$$A_{nn'}^{mm'}(1,2) = \frac{\pi}{2}\frac{[\varphi_n'(0,\omega_1)\varphi_{n'}'(0,\omega_1)\varphi_m'(0,\omega_2)\varphi_{m'}'(0,\omega_2)]}{[\kappa_n(\omega_1)\kappa_{n'}(\omega_1)\kappa_m(\omega_2)\kappa_{m'}(\omega_2)]^{1/2}} \times \int_{-\infty}^{\infty} d\Omega\, e^{-i\Omega\tau}\int_{-\infty}^{\infty} d\text{æ}_y\, e^{i\text{æ}_y\rho}F_\eta(\kappa_{nm}^{+} - \kappa_{n'm'}^{+}, \text{æ}_y, \Omega) \times e^{i(\kappa_{nn'}^{-}(\omega_1) - \kappa_{mm'}^{-}(\omega_2))x}$$

where $\kappa_{nm}^{+} = 0.5[\kappa_n(\omega_1) + \kappa_m(\omega_2)]$ and $F_\eta(\boldsymbol{\text{æ}}, \Omega)$ is the Fourier transform of the surface autocorrelation function $B_\eta(\rho, \tau)$ with respect to ρ and τ.

A considerable simplification occurs for the waveguides having a non-equidistant spectrum of wavenumbers κ_n. In this case, in the limit of large x, the diagonal elements of the matrix $\Gamma_{nm}(1, 2)$ decouple from the off-diagonal elements in (8). As a consequence, for Γ_{nm} at $n \neq m$, we have approximately [37]

$$\Gamma_{nm}(1,2) = \langle p_n(1)\rangle\langle p_m^*(2)\rangle T_{nm}(1,2), \quad n \neq m \tag{14}$$

where

$$\langle p_n(\mathbf{r}, \omega, t)\rangle = \frac{-i\varphi_n(z_0, \omega)}{\sqrt{8\pi x}}e^{(i\kappa_n(\omega)|\mathbf{r}| - \frac{1}{2}\sigma_n(\omega) - i\frac{\pi}{4})}$$

is the coherent field of the nth mode, $\sigma_n(\omega) = A_{nn}(1, 1)$ is the scattering coefficient, and

$$T_{nm}(1,2) = \exp\left\{\int_0^x dx'\, A_{nm}^{nm}\left(\rho\frac{x}{x'}, \tau, \omega_1, \omega_2\right)\right\}.$$

For most oceanic applications, the characteristic correlation length l_η of surface irregularities is much less than the typical mode cycle distance, i.e., $l_\eta \ll \Lambda_n$. In this case, elementary acts of scattering occur at statistically independent ensembles of the surface, and (14) reduces to a simpler form [18]

$$\Gamma_{nm}(1,2) = \langle p_n(1)\rangle\langle p_m^*(2)\rangle, \quad n \neq m. \tag{15}$$

For the diagonal elements $\Gamma_{nn}(1, 2)$, a formal procedure similar to that given in obtaining (11) leads to the expression [37]

$$\Gamma_{nn}(1,2) = \frac{1}{2\pi}\sum_{m=1}^{M}\Gamma_{mm}^0(1,2)\int_0^{2\pi} d\alpha\, e^{-i(n-m)\alpha - \frac{1}{2}D_m^\alpha(1,2)} \tag{16}$$

where $\Gamma_{mm}^0(1, 2)$ are the self-modal functions in the absence of random scattering and

$$D_m^\alpha(1,2) = \frac{\pi}{2}\frac{\varphi_m'(0,\omega_1)\varphi_m'(0,\omega_2)}{\sqrt{\kappa_m(\omega_1)\kappa_m(\omega_2)}}\sum_{q=1}^{M}\frac{\varphi_q'(0,\omega_1)\varphi_q'(0,\omega_2)}{\sqrt{\kappa_q(\omega_1)\kappa_q(\omega_2)}} \times \int_0^x dx' \int_{-\infty}^{\infty} d\Omega \int_{-\infty}^{\infty} d\text{æ}_y F_\eta(\kappa_m - \kappa_q, \text{æ}_y, \Omega) \times \left[1 - \cos\left(\text{æ}_y\rho\frac{x'}{x}\right)\cos(\Omega\tau)e^{i(q-m)\alpha}\right].$$

Equations (15) and (16) together with (7) allow for estimation of the key correlation characteristics of the acoustic signal in an upper sound channel where the rough surface scattering effects are important.

III. Coherence-Reduced Signal Processing in Large Arrays

In this section, we give a short introduction to array processing of partially coherent or spatially random signals, which is then supported (see Section IV) by the numerical results on array beamforming in deep-water environments from the Northwest Pacific. Our analysis is aimed at examining the array gain and its coherence-induced loss for optimal beamformers, including linear and quadratic.

A. Background

Generally, the problem of array signal processing is to detect a signal source and/or to estimate unknown source or transmission parameters. In both cases, one possible strategy is to optimally process the outputs of array elements (sensors) according to a predetermined statistical criterion. In this respect, the ML processor is well known to be of fundamental importance because it is optimal for a variety of detection and estimation criteria [7], [8].

Conventional array beamformers such as those used for plane-wave source detection or bearing estimation in radar

[38], [39] are derived under the key assumptions of a time-invariant and spatially homogeneous transmission channel between a source and sensors. In long-range sonar applications, however, such model assumptions are generally unrealistic. Therefore, two principal issues arise: 1) the effects of signal propagation in a deterministically inhomogeneous channel and 2) the effects of random inhomogeneities which perturb a regular wavefield and cause its coherence loss.

A survey of the literature reveals that several important developments have been made in these directions. First, a technique of matched-field processing (MFP) was proposed [40] and intensively studied as an effective generalization of plane-wave beamforming with applications to the source localization in underwater channels and ocean acoustic tomography [41]–[42]. Second, a general theory of array signal processing in regular multimode/multipath channels was developed with applications to the detection problem in underwater acoustics [43]. Third, the coherence effects on the array beampattern [44], [45] and the detection performance [3]–[6] were examined by the use of some models of plane-wave signal coherence. Finally, more relevant models of the multimode signal coherence were used to predict the array beampattern degradation [46] and to compare SNR loss for several linear and quadratic beamformers, the optimal ones included [12]–[14], [47], [48].

Thus, recent developments of array signal processing in random-inhomogeneous multimode channels lay the theoretical background of our study concerned with signal coherence effects on large-array beamforming.

B. Preliminary Formulations

The problem of array signal processing under the conditions of reduced signal coherence was clearly formulated and studied by Cox [3] and was then elaborated by other authors [4]–[6], [49], [50] on the basis of a general theory of random signal detection [7], [8]. Following these works, we outline below basic formulations for the optimal large-array processing of partially coherent signals with emphasis on small-signal consideration.

The signal of interest and the noise background are both assumed to be zero-mean, mutually uncorrelated, and Gaussian random processes. The detection problem is formulated as a two-hypothesis alternative

$$\mathbf{x}=\mathbf{s}+\mathbf{n} \quad \text{or} \quad \mathbf{x}=\mathbf{n}$$

where $\mathbf{s}$ and $\mathbf{n}$ are, respectively, the N-dimensional signal and noise vectors of the Fourier-transformed data vector $\mathbf{x}$ received by the N-element array. In the numerical simulations following in Section IV, the components of the signal vector are exactly the acoustic pressures from (1), i.e., $s_j = P(\mathbf{r}_j, z_j, t)$, $j = 1, 2, \cdots, N$.

In general, the data vector $\mathbf{x}$ can be processed in quadratic form to obtain the detection statistic d by

$$d=\mathbf{x}^T\mathbf{A}\mathbf{x}^* \tag{17}$$

where $\mathbf{A}$ is an arbitrary $(N\times N)$ matrix and the superscript "T" denotes transpose. For the ML criterion, the optimal matrix $\mathbf{A}_{\text{opt}}$ is expressed by

$$\mathbf{A}_{\text{opt}}=\mathbf{\Gamma}_n^{-1}-(\mathbf{\Gamma}_s+\mathbf{\Gamma}_n)^{-1}.$$

Here, $\mathbf{\Gamma}_s$ and $\mathbf{\Gamma}_n$ are the spatial covariance matrices of the signal and noise, respectively, which are defined for a random vector $\mathbf{x}$ as $\mathbf{\Gamma}_x = \langle \mathbf{x}\mathbf{x}^+ \rangle$ (the superscript "$+$" denotes conjugate transpose).

Under the small-signal condition, which is a reasonable assumption for long-range underwater acoustics and will be used in further analysis, the detection performance can be characterized by the deflection q of the detection statistic d. The deflection, also known as the detection index or generalized SNR, is given by

$$q=\frac{\langle d(\mathbf{s}+\mathbf{n})\rangle-\langle d(\mathbf{n})\rangle}{(\langle d^2(\mathbf{n})\rangle-\langle d(\mathbf{n})\rangle^2)^{1/2}}. \tag{18}$$

The optimal small-signal matrix $\mathbf{A}_{\text{opt}}$ and deflection q_{opt} are given, respectively, by

$$\mathbf{A}_{\text{opt}}=\mathbf{\Gamma}_n^{-1}\mathbf{\Gamma}_s\mathbf{\Gamma}_n^{-1} \tag{19}$$

$$q_{\text{opt}}=\left[\text{Tr}\left(\mathbf{\Gamma}_n^{-1}\mathbf{\Gamma}_s\right)^2\right]^{1/2}. \tag{20}$$

An important point is the fact that (19) and (20) can be derived alternatively by directly maximizing the deflection q [see (18)] for arbitrary signal statistics. Therefore, the choice of the maximum deflection criterion is quite reasonable in the situation of weak and unknown (non-Gaussian) signals in the Gaussian noise background, when the ML criterion is generally not applicable to give the optimal processor [8].

The components of (18) vary with the signal and noise power (since q itself depends quadratically on the components s_j and n_j, $j = 1, 2, \cdots, N$). Therefore, the deflection (18) can be used to compare directly the array gain and the gain loss for different beamformers. The array gain G is defined as the deflection, or the output SNR q normalized to the input SNR q_0, and the gain loss δ as the gain normalized to the number of array elements

$$G=\frac{q}{q_0}, \quad q_0=\frac{\text{Tr}(\mathbf{\Gamma}_s)}{\text{Tr}(\mathbf{\Gamma}_n)}, \quad \delta=\frac{G}{N} \tag{21}$$

(the symbol $\text{Tr}(\cdot)$ denotes the matrix trace). Concerning the array gain definition, we point out that the input SNR q_0 is defined here as the ratio of the signal and noise intensities which are spatially averaged over the array length.

The detailed predictions of the array gain and gain loss from (21) are of our primary interest to examine the large-array signal processors in long-range underwater environments.

C. Array Beamformers

A general structure of a quadratic beamformer (QBF) can be described clearly using the processor matrix $\mathbf{A}$ (17) in factorized form as $\mathbf{A}=\mathbf{W}\mathbf{W}^+$, where $\mathbf{W}$ is an $(N\times R)$ weight matrix consisting of vector-rows $\mathbf{w}_p$ $(p = 1, 2, \cdots, R, 1 \le R \le N)$. This structure consists, therefore, of the matrix filter $\mathbf{W}$ followed by an R-channel quadratic processor. Its weight-square-sum output y_{QBF} is obtained directly as a *quadratic*

function of the input vector $\mathbf{x}$ by

$$y_{\mathrm{QBF}} = d = |\mathbf{W}^T\mathbf{x}|^2 = \sum_{p=1}^{R} \left|\mathbf{w}_p^T\mathbf{x}\right|^2. \tag{22}$$

The output SNR q_{QBF} is obtained from (18) by

$$q_{\mathrm{QBF}} = \frac{\mathrm{Tr}(\mathbf{W}^T\mathbf{\Gamma}_s\mathbf{W}^*)}{[\mathrm{Tr}(\mathbf{W}^T\mathbf{\Gamma}_s\mathbf{W}^*)^2]^{1/2}}. \tag{23}$$

Each partial channel of QBF (22) is a linear beamformer (LBF) characterized by the corresponding weight vector $\mathbf{w}_p$ $(p = 1, 2, \cdots, R)$. To distinguish from QBF, the LBF weight-sum output y_{LBF} is obtained as a *linear* function of the input vector $\mathbf{x}$, and the detection statistic d as a squared y_{LBF} by

$$y_{\mathrm{LBF}} = \mathbf{w}^T\mathbf{x}, \quad d = |\mathbf{w}^T\mathbf{x}|^2 \tag{24}$$

where $\mathbf{w}$ is an arbitrary $(N \times 1)$ weight vector. The output SNR q_{LBF} is given by the following ratio:

$$q_{\mathrm{LBF}} = \frac{\mathbf{w}^T\mathbf{\Gamma}_s\mathbf{w}^*}{\mathbf{w}^T\mathbf{\Gamma}_n\mathbf{w}^*}. \tag{25}$$

Thus, the LBF structure gives a vector filter $\mathbf{w}$ followed by a single-channel quadratic detector. This is a conventional choice for array signal processing with numerous applications in radar and sonar.

General structures of the LBF and QBF, as they follow directly from (24) and (22), respectively, are shown in Fig. 1.

Comparing these structures, we conclude that the QBF scheme is an incoherent (squared) combination of R partial LBF's and reduces to the linear scheme in the particular case of $R = 1$. A choice of the weight vector $\mathbf{w}$ and matrix $\mathbf{W}$ in the LBF and QBF schemes, respectively, directly determines the output processor performances for given signal and noise covariance matrices.

We turn now to the optimal quadratic and linear beamformers which are then used in Section IV to examine the coherence-induced effects on large-array signal processing in deep water.

For the optimal QBF derived from (19)–(22), the partial weight vectors $\mathbf{w}_p$ and SNR q_{opt} are given by

$$\mathbf{w}_p^* = \lambda_p^{1/2}\mathbf{\Gamma}_n^{-1}\mathbf{m}_p, \quad q_{\mathrm{opt}} = \left\{\sum_{p=1}^{r} q_p^2\right\}^{1/2} \tag{26}$$

where λ_p and $\mathbf{m}_p$ are the eigenvalues and eigenvectors of the signal matrix $\mathbf{\Gamma}_s$, respectively, and the quantities q_p are determined below. The eigenvalues λ_p are assumed to be ordered and normalized by

$$\lambda_1 \geq \lambda_2 \geq \cdots \lambda_r > 0, \quad r = \mathrm{rank}(\mathbf{\Gamma}_s), \quad \sum_{p=1}^{N} \lambda_p = 1. \tag{27}$$

As follows from (26), the number R of partial LBF's in the optimal QBF is exactly the signal rank r. Therefore, the linear structure can be optimal if and only if the signal matrix $\mathbf{\Gamma}_s$ is the rank-one matrix. This conclusion is extremely important for our study because the signal coherence and the signal rank are intrinsically interrelated: the rank r increases with the array length N as compared to the coherence length N_c (where N_c is the dimensionless coherence length expressed in element spacing units), i.e., with the increase of the N/N_c ratio.

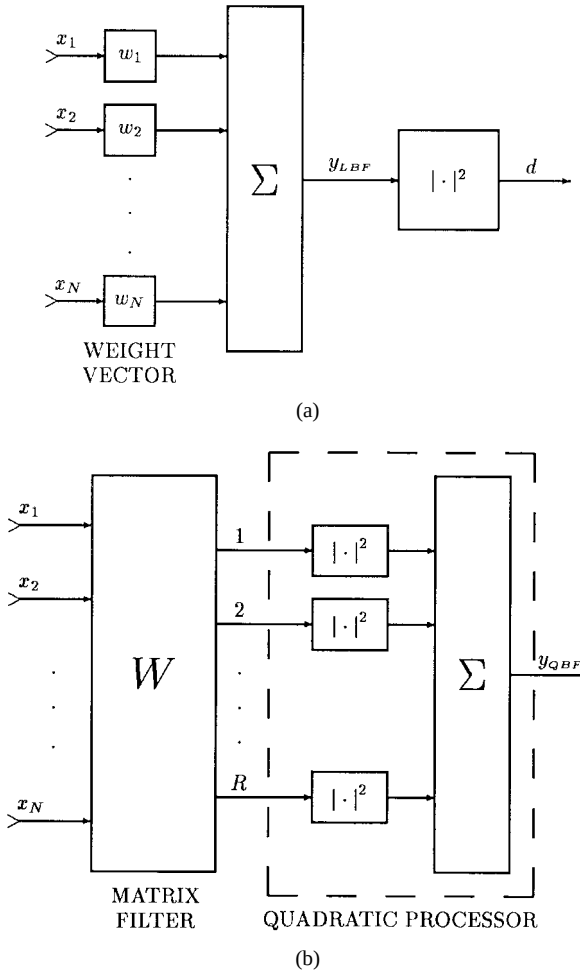

Fig. 1. A general structure of (a) linear and (b) quadratic beamformers.

Of particular interest is the optimal linear processor which exhibits the ultimate coherence-induced limitation for all possible LBF's [in other words, for all possible vectors $\mathbf{w}$ in (24) and (25)]. Its weight vector and SNR are given by the following eigenvalue–eigenvector problem:

$$q_p\mathbf{v}_p = \mathbf{\Gamma}_n^{-1}\mathbf{\Gamma}_s\mathbf{v}_p, \quad p = 1, 2, \cdots, r = \mathrm{rank}(\mathbf{\Gamma}_s). \tag{28}$$

The largest eigenvalue q_1 gives the maximum SNR q_{LBF} (25), and the corresponding eigenvector $\mathbf{v}_1$ gives the optimal weight vector $q_{\mathrm{LBF}} = q_1$, $\mathbf{w}_{\mathrm{opt}} = \mathbf{v}_1^*$. Moreover, the eigenvalues q_p from (28) give the optimal SNR q_{opt} [see (20) and (26)].

It follows from (26) and (28) that, in the case of the rank-one signal matrix emphasized above, both the optimal QBF and LBF reduce to the steady-state adaptive beamformer [38], [39] which is, therefore, the optimal scheme to process the perfectly coherent signal against the noise interference. Its weight vector is given by

$$\mathbf{w}^* = \mathbf{\Gamma}_n^{-1}\mathbf{s}. \tag{29}$$

This well-known equation derives the noise prewhitening beamformer followed by the matched-signal filter.

For the purpose of emphasizing the signal coherence effect, we point out a particular case of spatially white noise. In this case, the optimal QBF scheme is the incoherent λ_p-weighted combination of the partial filters matched to the signal eigencomponents $(\lambda_p, \mathbf{m}_p)$ from (26), while the optimal LBF matches the first (most powerful) eigencomponent $(\lambda_1, \mathbf{m}_1)$. Therefore, an additional gain Q of the optimal QBF over the optimal LBF is determined only by the signal eigenvalues

$$Q = \frac{G_{\mathrm{QBF}}}{G_{\mathrm{LBF}}} = \frac{\left(\sum_{p=1}^{r} \lambda_p^2\right)^{1/2}}{\lambda_1}, \quad 1 \le Q \le r^{1/2}. \tag{30}$$

In practice, only the largest eigenvalues and an "effective" rank r_{eff} (defined as their number) are of real importance for estimation of the quadratic processor performance, while the contribution of the higher order eigenvalues λ_p (with the numbers $p > r_{\mathrm{eff}}$) can be ignored.

Thus, the following characteristics of the received signal are of the greatest importance with application to the optimal large-array processors: the first (largest) eigenvalue λ_1, the effective rank r_{eff}, and the quadratic gain Q from (26)–(30). All of them are determined by the signal eigenvalues and, therefore, are intrinsically interrelated.

The physical parameter related to the signal eigenvalues is the ratio N_c/N which can be estimated by direct measurements using the array. For the case of a coherence-degraded signal, $N_c/N \ll 1$, the following estimates are of interest:

$$\lambda_1 \sim \frac{N_c}{N}, \quad r_{\mathrm{eff}} \sim \frac{N}{N_c}, \quad Q \sim r_{\mathrm{eff}}^{1/2} \sim \left(\frac{N}{N_c}\right)^{1/2}. \tag{31}$$

The general formulations outlined above have been effectively exploited by several authors to simulate the optimal processors and to consider suboptimal (quadratic and linear) techniques by the use of exponential-type models for the signal MCF [3]–[6], [49]. In our papers [47], [48], [50], the theory has been developed by incorporating a model of multimode signal coherence and simulations of the modal covariance effects on array beamforming. Two intrinsic factors, the modal covariances and the mode orthogonality, were shown to affect mutually optimal array beamforming and detection performance. For example, the signal rank r is considerable, $r \sim M$, if the signal-carrying modes (M is their number) are weakly correlated and the array length is sufficient for their shapes orthogonality or spatial resolution.

In this paper, the effects of ocean acoustic coherence on the array gain are compared for the following four beamforming techniques.

1) Plane-Wave Beamformer (PWBF): This is the simplest processor of the steered array. The entries of its weight vector $\mathbf{w}_{\mathrm{PW}}$ are given by

$$w_{\mathrm{PW}}(j) = \exp[-ikd(j-1)\sin\beta], \quad j = 1, 2, \cdots, N \tag{32}$$

where β is the steering angle (arbitrary). The steering angle is the only parameter of the PWBF which is changed to control the output SNR and gain.

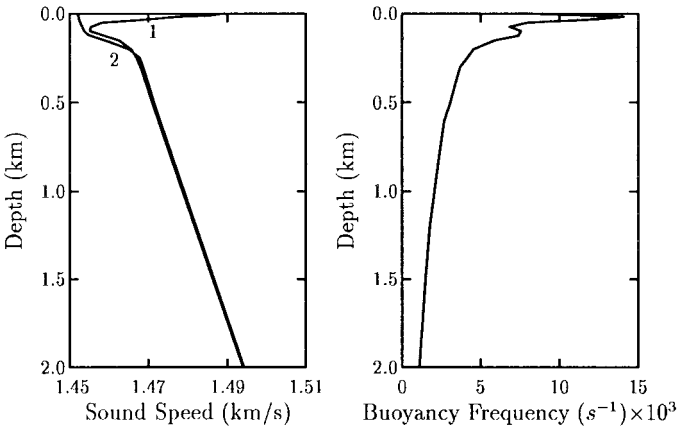

Fig. 2. Upper parts of (a) sound-speed profiles and (b) buoyancy distribution from the Northwest Pacific. The profiles are: summer (1), winter (2).

2) Adaptive PWBF: This is the PWBF with noise interference prewhitening [38], [39]. Its weight vector $\mathbf{w}_{\mathrm{APW}}$ [see also (29)] is given by

$$\mathbf{w}_{\mathrm{APW}} = \mathbf{\Gamma}_n^{-1}\mathbf{w}_{\mathrm{PW}} \tag{33}$$

and its SNR q_{APW} is obtained by direct substitution of $\mathbf{w}_{\mathrm{APW}}$ into (25).

3) Optimal LBF: This beamformer was given above:

$$\mathbf{w}_{\mathrm{opt}} = \mathbf{v}_1^*, \quad q_{\mathrm{LBF}} = q_1 \tag{34}$$

where q_1 and $\mathbf{v}_1$ are, respectively, the largest eigenvalue and the corresponding eigenvector from (28).

4) Optimal QBF: This is a full-optimal beamformer from (19), (20), (26)

$$\mathbf{W}_{\mathrm{opt}}\mathbf{W}_{\mathrm{opt}}^{+} = \mathbf{A}_{\mathrm{opt}}, \quad q_{\mathrm{QBF}} = q_{\mathrm{opt}}. \tag{35}$$

Obviously, the first three techniques follow from the linear structure in Fig. 1(a) and the last technique from the quadratic structure in Fig. 1(b).

IV. Predictions of the Acoustic MCF with Application to Large-Array Performance Degradation

In this section, we give some illustrative examples to exhibit numerical predictions of: 1) the acoustic MCF for the given sound-speed profile and spectrum of oceanic inhomogeneities and 2) the coherence-induced effects on the array beampattern and SNR gain for both horizontal and vertical array configurations.

The two sound-speed profiles chosen for our calculations are shown in Fig. 2. They represent summer and winter seasonal averages and buoyancy frequency in the Northwest Pacific at latitude 45°N.

The sound scattering in the summer channel is caused mainly by volume fluctuations in the index of refraction and, in the winter channel, by contrast, by a stochastically rough surface. To illustrate the corresponding effects of random volume and surface scattering on acoustic transmission, we exploit the Garrett–Munk spectrum [35] for internal waves and the Pierson–Moskowitz spectrum [51] for surface wind waves.

The following set of parameters is used: source frequency $f_0 = 250$ Hz, distance $x = 250, 500, 1000$ km, source depth $z_0 = 50$ and 100 m, the horizontal array depth or the first element depth for the vertical array is 300 m, and the interelement distance for the arrays considered is 3 m.

A. Evaluations of the Acoustic MCF

We begin with observing the effect of medium fluctuations on the sound wavefield coherence. The calculations are concerned with the monochromatic case, when the frequency spectrum $g(\omega) = \delta(\omega - \omega_0)$.[2]

The coherence degree of the received signal is characterized by the correlation coefficient

$$C(\mathbf{r_1}, z_1, t_1 \mid \mathbf{r_2}, z_2, t_2) = \frac{\Gamma_s(\mathbf{r_1}, z_1, t_1 \mid \mathbf{r_2}, z_2, t_2)}{\sqrt{\Gamma_s(\mathbf{r_1}, z_1, t_1 \mid \mathbf{r_1}, z_1, t_1)\Gamma_s(\mathbf{r_2}, z_2, t_2 \mid \mathbf{r_2}, z_2, t_2)}} \tag{36}$$

where we have dropped the argument ω_0 for brevity. This function is fully determined by solutions of the eigenvalue problem [see (2)] and the RTE [see (8) and (9)].

1) Volume Scattering by Random Internal Waves: In Fig. 3, we plot the magnitude of the correlation coefficient from (36) in the case of transverse horizontal and vertical separations.

Calculations were carried out for the summer profile (curve 1 in Fig. 2) using the results of the work of Esswein and Flatte [36] for the phase-structure density from internal waves. It is evident from this figure that the characteristic coherence length, which is determined by the half-power decay of the correlation coefficient, decreases monotonically as the range increases.

2) Rough Surface Scattering by Fully Developed Seas: As was mentioned previously, surface interactions play a predominant role in acoustic signal fluctuations, when the propagation takes place in an upper sound channel (curve 2 in Fig. 2). For example, in the North Pacific, such situations exist perhaps 50% of the time in the winter.

For the case considered, the corresponding graphs for correlation functions are shown in Fig. 4. There is an additional environmental parameter, wind speed v, which varies here from 10 to 15 m/s. Obviously, the increase of the wind speed leads to the increase of rough surface scattering and coherence loss.

For moderate v ($v < 13$ m/s), the MCF of vertical separation behaves in an oscillatory fashion which indicates that the scattering is weak, so that there can be a rather high degree of coherence even at relatively large separation of the observation points. It should be emphasized that the normalized MCF tends asymptotically to the coherence parameter $I_c = |\langle P(\mathbf{r}, z, t)\rangle|^2 / \langle |P(\mathbf{r}, z, t)|^2 \rangle$. The characteristic coherence length time and in this case depends on wind speed and is $\sim$10 m for $v = 10$ m/s.

Thus, the signal coherence depends substantially on the receiving array configuration and on the source and environmental parameters. Based on these results, we demonstrate in Sections IV-B and -C that the long-range coherence loss causes significant degradation of the array beampattern and gain.

[2]Consideration of the nonmonochromatic case will be the subject of a separate paper aimed at studying temporal filtering of narrow-band acoustic pulses in a random oceanic waveguide.

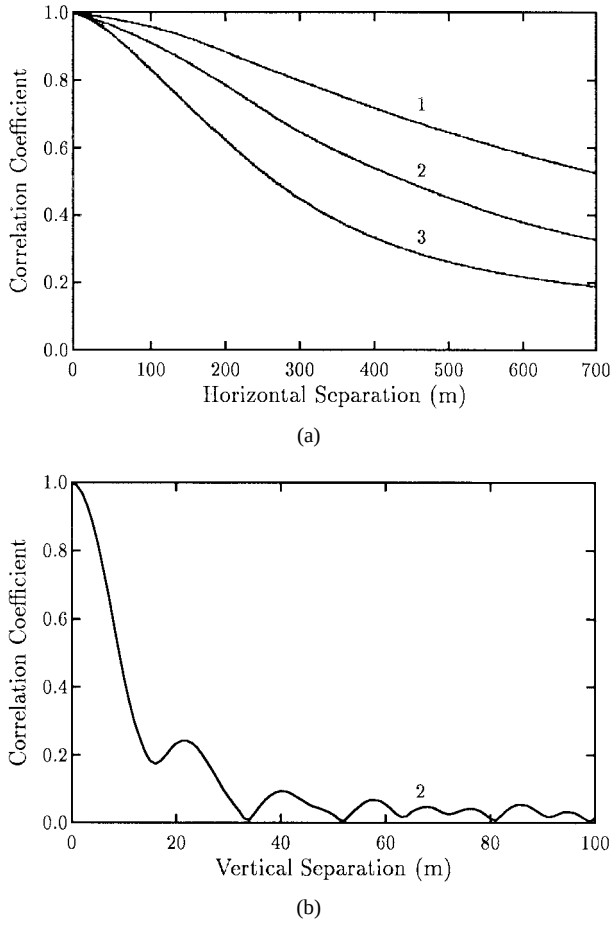

Fig. 3. The normalized MCF of (a) horizontal and (b) vertical separations in the summer environments at various ranges: 1: 250 km; 2: 500 km; 3: 1000 km. The source frequency is 250 Hz, the source depth is 50 m, and the depth of the horizontal array and the first element of the vertical array is 300 m.

B. Horizontal Array Gain Limitations

First, we give the results for the horizontal array configuration. In this example, the source is located at depth $z_0 = 100$ m, distance $x = 1000$ km, and direction $\alpha = 30°$.

For the main purpose of evaluating the signal coherence effects, the simulation is focused on the situation of a spatially white noise background, i.e., $\mathbf{\Gamma}_n = \mathbf{I}$ in the equations from Section III ($\mathbf{I}$ is the identity matrix). For calculations of the signal matrix $\mathbf{\Gamma}_s$, we exploit the respective MCF's of horizontal separations.

Fig. 5 shows the mean beampattern of the 256-element phased array as a function of the steering angle β in the (a) summer and (b) winter channels, respectively (curves 1 correspond to a regular channel in both cases).

The signal coherence loss is seen to lead to considerable degradation of the beampattern. This fact is generally well known [44], [45], but the pronounced feature is the main lobe angular displacement caused by modal broadening of the signal angular spectrum. This displacement leads to extremely high sensitivity of large-array PWBF to multimode

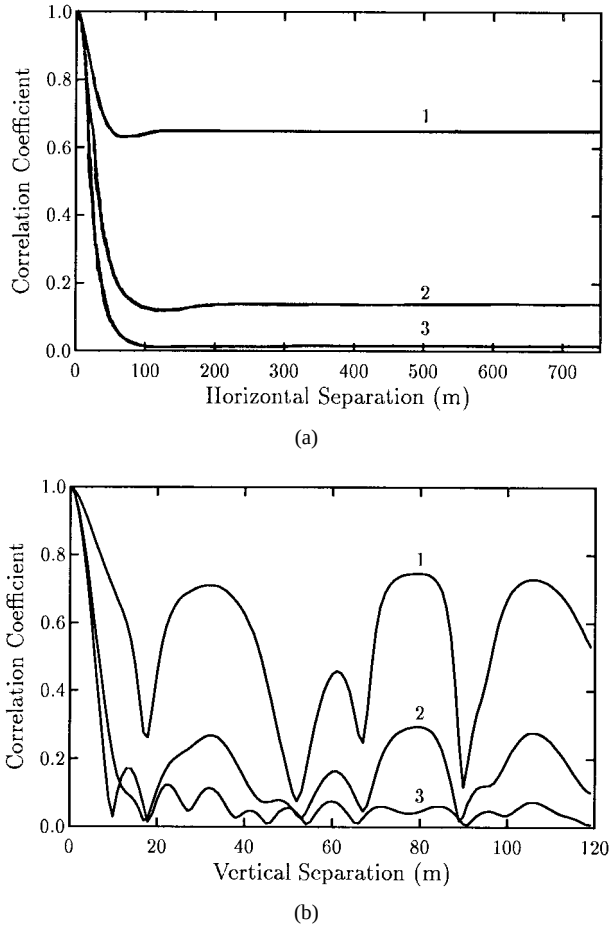

Fig. 4. The normalized MCF of (a) horizontal and (b) vertical separations in the winter environments at the range of 500 km and various surface roughness. 1: $v = 10$ m/s; 2: $v = 13$ m/s; 3: $v = 15$ m/s. The source frequency is 250 Hz, the source depth is 100 m, and the depth of the horizontal array and the first element of the vertical array is 300 m.

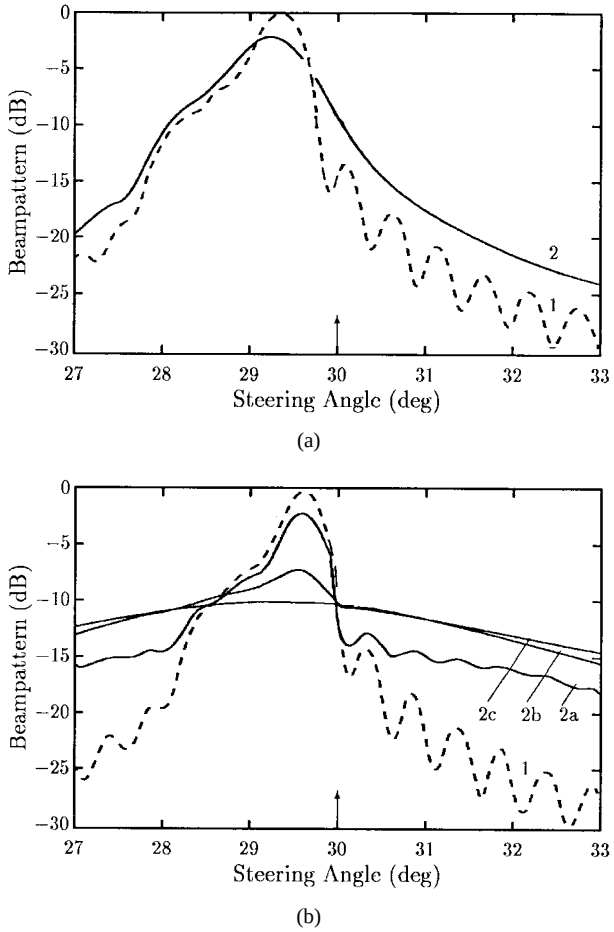

Fig. 5. Beampattern of the horizontal 256-element array in the (a) summer and (b) winter environments in the absence (1) and in the presence (2) of random inhomogeneities. 2a: $v = 10$ m/s; 2b: $v = 13$ m/s; 2c: $v = 15$ m/s. The arrow indicates the angle of arrival.

propagation even in a regular channel. Therefore, an adaptive correction of the main lobe direction is required to adjust the PWBF steering angle to the angular response maximum.

Fig. 6 shows the gain loss δ [see (21)] as a function of the number N of the array elements in the summer channel for the source direction $\alpha = 30°$.

A considerable degradation of the PWBF gain (for $\beta = \alpha$, see curve 4) is caused primarily by the main lobe displacement emphasized above. Note that the steep increase of the gain loss $\delta(N)$ for $N \gtrsim 50$ corresponds to the decreasing gain $G(N)$. The latter function achieves the maximum value $G \simeq 15$ dB for $N \simeq 50$ and shows a gradual decrease of the gain for larger arrays. It is seen that the angular correction required for such array lengths leads to the significant gain increase up to ~5–10 dB and achieves an almost LBF performance (see curves 2 and 3). On the other hand, this angular correction of PWBF does not entail any increase in computational complexity and has the essential advantage of environmental robustness.

Fig. 7 shows the same function $\delta(N)$ in the winter channel for the same angle $\alpha = 30°$ and two values of wind speed (a) $v = 10$ m/s and (b) $v = 15$ m/s. The curves in Fig. 7(a) are generally similar to those in Fig. 6 and illustrate, in particular, the angular dependence of the PWBF efficiency

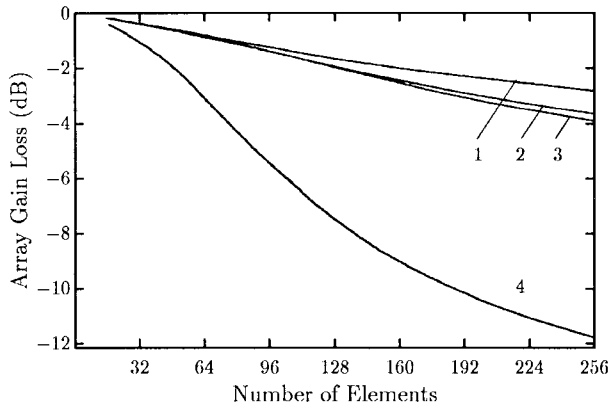

Fig. 6. Horizontal array gain loss in the summer environments as a function of the number of hydrophones. 1: optimal QBF; 2: optimal LBF; 3: PWBF with angular correction; 4: conventional PWBF.

that amounts up to ~10 dB. From Fig. 7(b), however, two essential conclusions concerned with fully developed wind waves follow. First, all the linear beamformers, the optimal LBF included, degrade in comparison with the optimal QBF with the increase of wind speed v; the additional quadratic gain Q [see (30)] is about 3 dB for the array length $N \sim 100$ and increases gradually with N. Second, the angular correction of

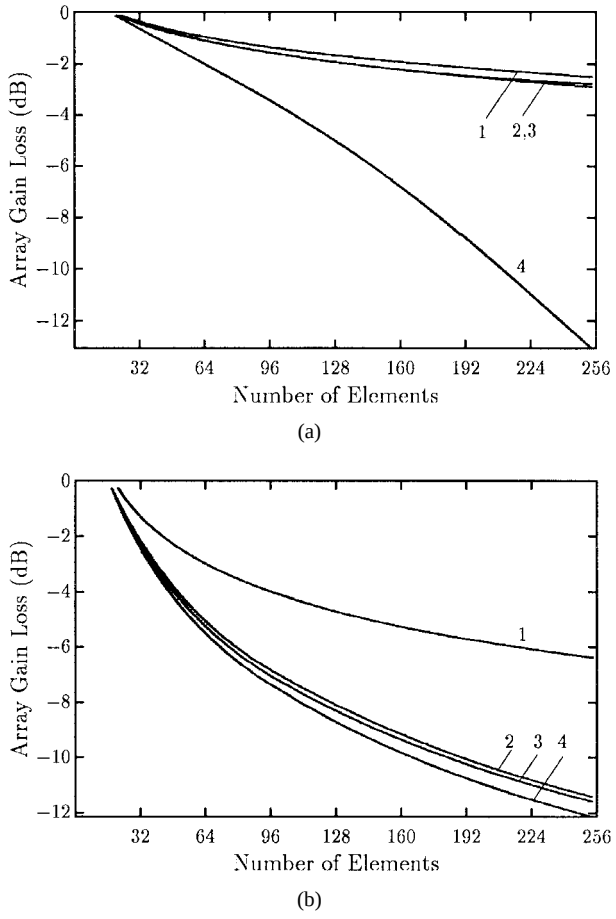

Fig. 7. Horizontal array gain loss in the winter environments as a function of the number of hydrophones for (a) $v = 10$ m/s and (b) $v = 15$ m/s. 1: optimal QBF; 2: optimal LBF; 3: PWBF with angular correction; 4: conventional PWBF.

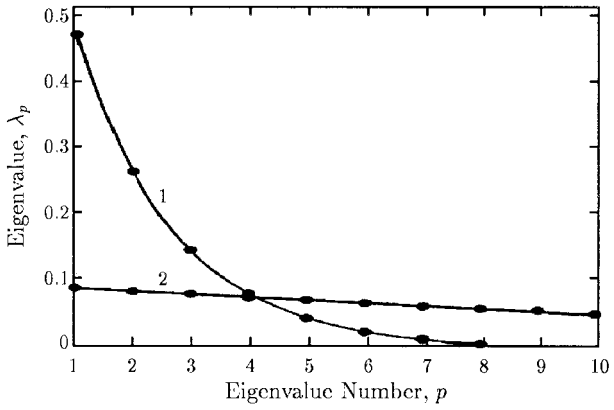

Fig. 8. Signal eigenvalues for the 256-element horizontal array in the summer (1) and winter (2) (at $v = 15$ m/s) environments.

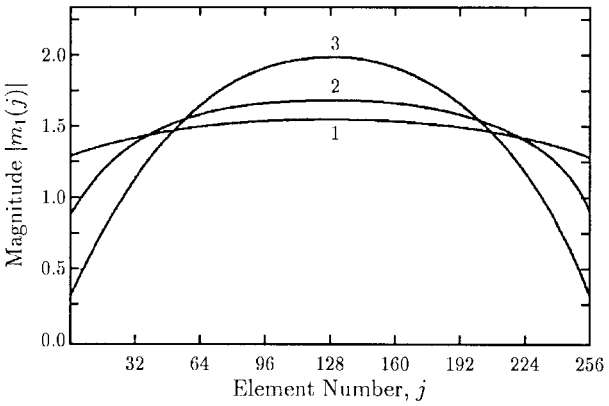

Fig. 9. Weight magnitudes for the 256-element horizontal array in the winter environments. 1: $v = 10$ m/s; 2: $v = 13$ m/s; 3: $v = 15$ m/s.

PWBF does not entail a significant effect on the array gain. A physical reason is rather clear, namely, the coherence length N_c is small compared to the array length N, $N_c/N \ll 1$ [see Fig. 4(a)]. This leads to: 1) an increase of the signal rank r and, therefore, to an increase of the "gap" between the optimal LBF and the QBF performances according to (30) and (31) and 2) almost complete degradation of the large-array beampattern [see Fig. 5(b)] and to consequent vanishing of the angular dependence of the PWBF performance.

To clarify the difference between the summer and winter conditions in more detail, we show in Fig. 8 the largest eigenvalues (27) of the covariance matrix $\mathbf{\Gamma}_s$ for $N = 256$ and $\alpha = 30°$. In the summer channel, the signal eigenvalues are seen to decrease rapidly with number p, and $r_{\text{eff}} \sim 3$. In the winter channel, on the contrary, the eigenvalue spectrum for $v = 15$ m/s is nearly uniform for the first numbers and $r_{\text{eff}} \sim 15$.

It is also of interest to compare in detail the array weights $w(j)$ for the PWBF with the angular correction and for the optimal LBF. These beamforming techniques, as is seen from Figs. 6 and 7, achieve almost the same gain performance. The reason is that the phase distribution of the first signal eigenvector $\mathbf{m}_1$ (which gives the weight vector for optimal LBF in the case of spatially white noise [see (28)] is very close to the phase distribution of the corrected PWBF array

$$\arg(m_1(j)) \simeq -kd(j-1)\sin\beta_{\max}$$

where $\beta_{\max}$ is the direction of maximum angular response from Fig. 5. The weight coefficients differ only by their magnitudes. For example, Fig. 9 shows the weight magnitudes for the 256-element array in the winter channel for three values of wind speed. These nonuniform windowing shapes entail some broadening of the optimal beampattern main lobe in comparison with the PWBF main lobe, which is caused by fluctuations of the modal angles of arrival.

Thus, we show that the coherence-induced effects on the horizontal array beampattern and gain are significant, especially in the winter environments of fully developed wind seas, and depend essentially on the beamforming technique used.

C. Vertical Array Gain Limitations

In this example, the source is located at depth $z_0 = 50$ m (for the summer channel) or $z_0 = 100$ m (for the winter channel) and distance $x = 500$ km.

The examination of vertical array processors includes also modeling of the ambient ocean noise. We assume, therefore, that the noise at the array inputs is the sum of spatially white

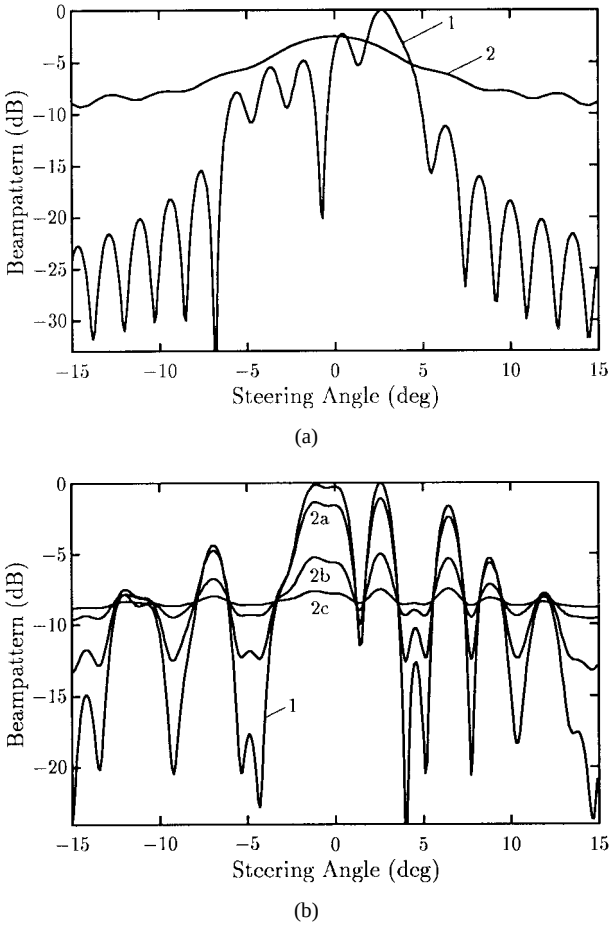

Fig. 10. Beampattern of the vertical 64-element array in the (a) summer and (b) winter environments in the absence (1) and in the presence (2) of random inhomogeneities. 2a: $v = 10$ m/s; 2b: $v = 13$ m/s; 2c: $v = 15$ m/s.

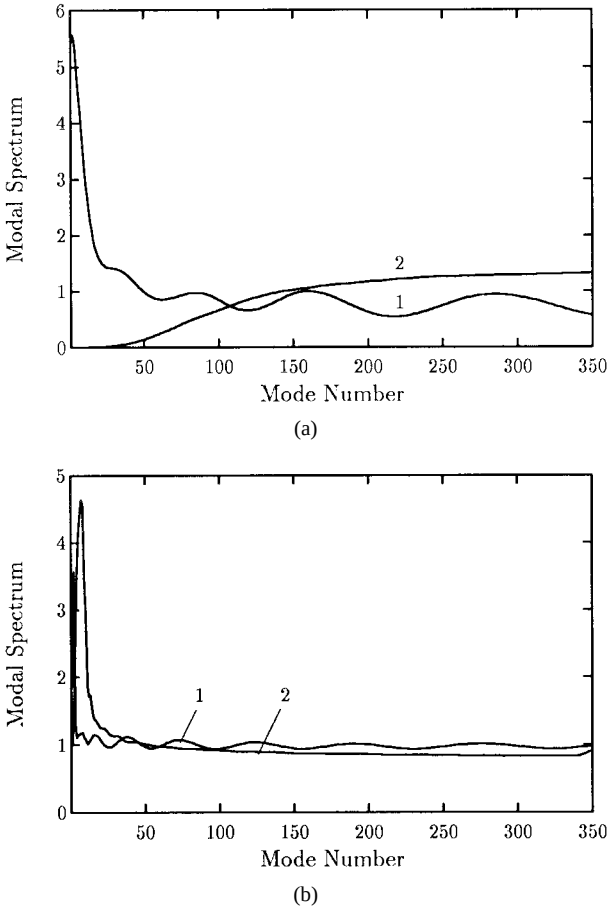

Fig. 11. Modal spectra of the signal (1) and ambient noise (2) in the (a) summer and (b) winter (at $v = 15$ m/s) environments. Modal spectra have been normalized to the area under their respective curves.

noise and ambient ocean noise

$$\mathbf{\Gamma}_n = \sigma \mathbf{I} + \mathbf{\Gamma}_{\text{an}} \tag{37}$$

where $\mathbf{I}$ is the identity matrix, $\mathbf{\Gamma}_{\text{an}}$ is the covariance matrix of ambient noise, and σ is a relative level of the white noise. The "vertical" matrix $\mathbf{\Gamma}_{\text{an}}$ is obtained from a widely used model of the ocean surface-generated noise [43], [52], according to which the noise is generated by uncorrelated sources with homogeneous spatial distribution over the ocean surface. This treatment is also based on the normal mode approach, so we interpret the ambient noise in (37) as the modal noise. As was previously estimated in [53], the modal noise effect on the vertical array gain depends inherently on "overlapping" of the signal and noise modal spectra.

To calculate the entries of the modal noise covariance matrix $\Gamma_{\text{an}}(i,j)$ $(i,j = 1,2,\cdots,N)$, we use the following equation [52]:

$$\Gamma_{\text{an}}(i,j) = \sum_{m=1}^{M} \frac{[\varphi'_m(0)]^2}{\kappa_m \operatorname{Im}(\kappa_m) H} \varphi_m(z_i)\varphi_m(z_j) \tag{38}$$

where $\varphi_m(z)$ and κ_m are, respectively, the modal depth functions and modal wavenumbers from (1).

To calculate the signal matrix $\mathbf{\Gamma}_s$, we exploit the respective MCF's from Figs. 3(b) and 4(b).

We examine here the array gain G [see (21)] instead of the gain loss δ. The reason is that modal noise prewhitening by the use of special techniques of matrix inversion [see (26), (28) and (33)] leads to some additional gain. This additional "noise" gain may be essential only if the modal noise is much more intensive in comparison with the white noise. It is this case that interests us in particular, so we suppose $\sigma = -20$ dB in (37).

Fig. 10 shows the 64-element array beampatterns in the (a) summer and (b) winter (b) channels. The beampatterns in both figures are plotted for comparison of regular and random-inhomogeneous channels (curve 1 corresponds to a regular channel). The signal coherence loss is seen to lead to a considerable degradation of the array beampattern, similar to the case of a large horizontal array (see Fig. 5). In both the channels, however, the maximum angular response corresponds to transverse propagation because the signal modal spectrum has a maximum in the lower order modes (see also curve 1 in Fig. 11).

Fig. 11 shows the modal spectra of the received signal and the ocean noise in the (a) summer and (b) winter channels. Comparison of these two cases shows that they differ essentially. In the summer channel, the noise power spectrum

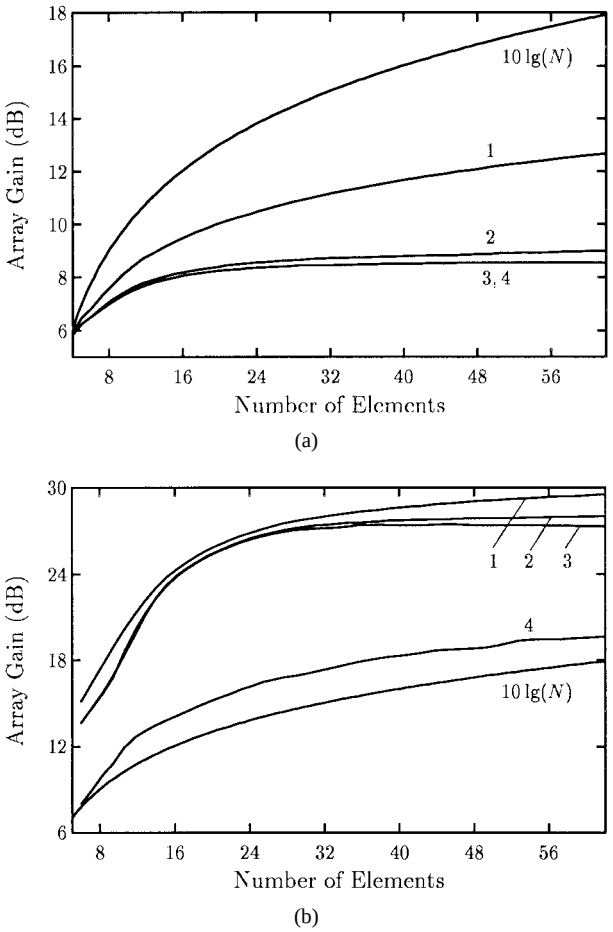

Fig. 12. Vertical array gain in the summer environment as a function of the number of hydrophones for (a) white noise and (b) modal noise. 1: optimal QBF; 2: optimal LBF; 3: adaptive PWBF; 4: PWBF.

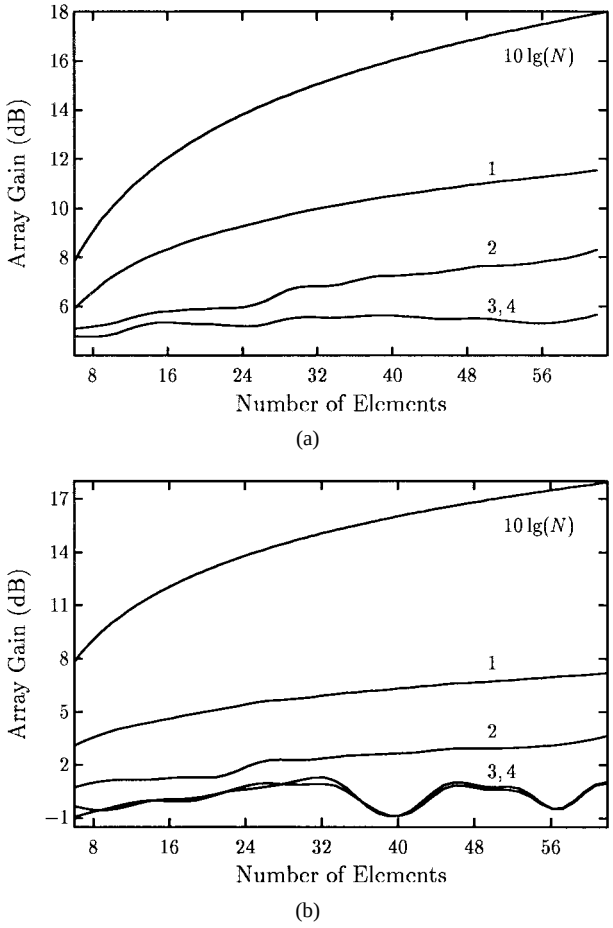

Fig. 13. Vertical array gain in the winter (at $v = 15$ m/s) environment as a function of the number of hydrophones for (a) white noise and (b) modal noise. 1: optimal QBF; 2: optimal LBF; 3: adaptive PWBF; 4: PWBF.

has a smooth maximum in the higher order ($m \gtrsim 100$) modes, so the signal and noise are localized mainly in different groups of modes. This fact leads to a general possibility of highly efficient modal noise suppression, which obviously corresponds to the particular case of transverse signal reception and modal interference reception in the sidelobe domain. The opposite situation is realized in the winter channel owing to the noise power localization in the lower order modes. This difference leads to a dramatic effect on the array gain [53] which is illustrated below.

Fig. 12 shows the array gain function $G(N)$ in the summer channel for the (a) white noise and (b) modal noise backgrounds. Since the main lobe is not displaced from the transverse direction ($\beta_{\max} = 0^{\circ}$), we plot only three gain functions in Fig. 12(a). A considerable increase of the gain in the case of modal noise (as compared to the case of white noise) is about 10–20 dB for all the beamformers. The most significant increase is seen to be achievable for the beamforming techniques which prewhite the modal noise. A considerable gain increase for a conventional PWBF is also due to angular selection of the signal by narrowing the beampattern main lobe and increasing the number of array elements.

Fig. 13 shows the array gain function $G(N)$ in the winter channel for the wind speed $v = 15$ m/s and the same two cases of the noise background. For the modal noise, the gain is seen to decrease (down to about -5 dB) for all the beamformers owing to similarity of the signal and noise modal spectra, which was emphasized above [see Fig. 11(b)]. Only the optimal large-array QBF achieves in this case a significant gain $G \sim 5$–7 dB. Moreover, the PWBF does not achieve any pronounced gain for all array lengths, so this technique is ineffective under these conditions.

Thus, the estimates of the vertical array gain vary, essentially depending not only on the signal coherence loss but also on the ambient noise modal spectrum. Moreover, the latter dependence can be even more pronounced and may lead to a dramatic effect, especially in the case of similar modal (angular) spectra of the signal and ambient noise.

V. Discussion and Conclusions

In this section, we conclude our study of the coherence effects on large-array signal processing in long-range deep-water environments and summarize the key results obtained.

The MCF is of great importance for understanding the statistical behavior of ocean acoustic transmission. It was shown how to efficiently derive an asymptotic expression for the MCF in terms of modal structure of the acoustic pressure field using the RTE. The method for solving the corresponding

matrix equation is based on a combined use of the WKB approximation and the generating function technique. The procedure elaborated on here allows one to reduce the problem of the wavefield coherence calculation in a refractive sound channel with random volume inhomogeneities to the analogous problem in free space. The method employed was also extended to include rough surface scattering effects. The application is illustrated by numerical computation of the expected acoustic coherence for deep-water ocean environments under the assumption that the random field of either internal waves or fully developed seas is the dominant source of transmission fluctuations.

Rough surface scattering was found to cause the most significant effects on ocean acoustic coherence. In particular, as observed in the results of Section IV, for a source of 250 Hz and at a range of 500 km, the horizontal coherence length varies from $\sim$400 m (in the summer conditions) to $\sim$40 m (in the winter conditions, $v = 15$ m/s), and the respective vertical coherence length varies from $\sim$10 m to $\sim$5 m.

We have presented calculations of internal wave and surface wind wave effects. Of course, other ocean processes are also possible. For example, the ocean variability due to mesoscale eddies or mean currents will cause acoustic variations but will not affect the coherence we are studying at long ranges and low frequencies (see, e.g., [54]).

Measurements of horizontal and vertical coherence have been carried out in many experiments. Ample data have been collected in the book by Stefanick [55]. The majority of the data indicates that typical measures of coherence lengths are 10 to 100 wavelengths for horizontal separations and less than 10 wavelengths for vertical separations. Our respective calculations are in good agreement with these experimental results.

Thus, we can conclude from this study that the RTE technique is a powerful tool for calculating acoustic propagation in a medium where random scattering effects are important. It is clear, however, that more accurate oceanographic measurements taken simultaneously with acoustic measurements will be required for comparison with our theoretical expressions. More recent experiments have been conducted under the SLICE89 and the ATOC projects, for which detailed environmental data are available. The application of the multimodal RTE to these data will be another interesting test of the technique. The RTE method could also be applied to treat: 1) combined effects of volume and rough surface scattering: 2) pulse signal propagation; and 3) the MCF behavior in shallow water where bottom interactions are essential.

The effect of oceanic fluctuations on the received signal coherence was shown to be of the greatest importance in application to large-array beamforming. The following three factors were shown distinctly to be the key points: 1) modal spreading of the received signal angular spectrum; 2) multimode signal coherence degradation; and 3) ambient noise directionality. The particular effects of these factors depend intrinsically on the array configuration in a channel and the array length. Moreover, the beamforming techniques were shown to be very different from the point of view of environmental robustness.

The PWBF technique was shown to be the most "sensitive" to factors 1)–3). This means that the PWBF gain can dramatically vary as a function of the source and environmental parameters. Of primary importance is the fact that adaptive correction of the steering angle can lead to an essential improvement of the performance. For example, for the horizontal array length of about 100λ, this gain increase was demonstrated to be up to $\sim$10 dB. The possibility of maintaining the PWBF efficiency is firmly restricted, however, by the cases of: 1) "residual" signal coherence over the full array length and 2) partial separation of the modal spectra of the signal and noise interference. These two cases are generally independent of each other but mutually affect the large-array gain.

An obvious advantage of the PWBF techniques is their comparative simplicity. They do not require a preprocessing procedure to estimate the signal eigenspace, and their performance can easily be controlled by reforming the beampattern, including adaptive angular correction of the main lobe.

As distinct from the PWBF, the optimal processing techniques require the signal eigenvalue–eigenvector analysis. To synthesize the optimal LBF and QBF schemes, one needs, therefore, to estimate the signal eigenspace in the noise background. The full-optimal QBF reduces significantly the coherence-induced gain loss, however, at a cost of increased processor complexity; the number of its partial weight-sum channels is equal to the number of the largest signal eigenvalues, as compared to the linear beamformers which require only one weight-sum channel. The reason for following such a complicated scheme is only the long-range signal coherence degradation, namely, the small values of the ratio $N_c/N \ll 1$, or, in other words, the case of $r_{\text{eff}} \gg 1$. Under these conditions, the additional quadratic gain Q [see (30)] is considerable, $Q \sim r_{\text{eff}}^{1/2}$, and its value was shown to be $\sim$3–6 dB.

Therefore, *a priori* estimation [see (31)] is the key point of the optimal processor performance/complexity analysis in the coherence-degraded situations. The most essential and pronounced feature of the optimal QBF is the increase of the gain function $G(N)$ for all array lengths N without a "saturation" plateau. The latter, in turn, is an intrinsic feature of the optimal LBF.

In conclusion, we summarize that: 1) the large-array gain performance in long-range ocean environments is inherently limited by the spatial coherence of multimode acoustic signal and 2) the full potential of large arrays will not be realized unless the coherence characteristics are known in detail and incorporated into signal processing.

REFERENCES

[1] S. M. Flatte, R. Dashen, W. H. Munk, K. M. Watson, and F. Zachariasen, *Sound Transmission Through a Fluctuating Ocean*. Cambridge, U.K.: Cambridge Univ., 1979.

[2] L. M. Brekhovskikh and Yu. P. Lysanov, *Fundamentals of Ocean Acoustics*. Berlin, Germany: Springer-Verlag, 1982.

[3] H. Cox, "Line array performance when the signal coherence is spatially dependent," *J. Acoust. Soc. Amer.*, vol. 54, pp. 1743–1746, 1973.

[4] A. M. Vural, "Effects of perturbations on the performance of optimum/adaptive arrays," *IEEE Trans. Aerosp. Electron. Syst.*, vol. AES-15, pp. 76–87, 1979.

[5] R. Laval and Y. Labasque, "Medium inhomogeneities and instabilities: Effects on spatial and signal processing," in *Underwater Acoustics and Signal Processing*, L. Bjørno, Ed. Dordrecht, The Netherlands: Reidel, 1981, pp. 41–70.

[6] D. R. Morgan and T. M. Smith, "Coherence effects on the detection performance of quadratic array processors, with application to large-array matched-field beamforming," *J. Acoust. Soc. Amer.*, vol. 87, no. 2, pp. 737–747, 1990.

[7] H. L. Van Trees, *Detection, Estimation and Modulation Theory, Part I*. New York: Wiley, 1968.

[8] C. R. Baker, "Optimum quadratic detection of a random vector in gaussian noise," *IEEE Trans. Commun.*, vol. COM-14, pp. 802–805, June 1966.

[9] A. G. Sazontov, "Acoustic coherence in a deep random oceanic waveguide," in *Formation of Acoustical Fields in Oceanic Waveguides*, V. I. Talanov and V. A. Zverev, Eds. Nizhny Novgorod, Russia: Institute of Applied Physics, 1995, pp. 37–62.

[10] A. G. Sazontov, "Quasiclassical solution of the radiation transport equation in a scattering medium with regular refraction," *Acoust. Phys.*, vol. 42, no. 4, pp. 487–494, 1996.

[11] A. G. Sazontov and N. K. Vdovicheva, "Modeling low-frequency sound scattering in a random oceanic waveguide using a modal formulation," in *Proc. 3rd Eur. Conf. on Underwater Acoustics*, Heraklion, Greece, 1996, vol. 1, pp. 133–138.

[12] E. Yu. Gorodetskaya, A. I. Malekhanov, A. G. Sazontov, and V. A. Farfel', "Effects of long-range sound propagation in random ocean on horizontal array gain loss," *Acoust. Phys.*, vol. 42, no. 5, pp. 543–649, 1996.

[13] E. Yu. Gorodetskaya, A. I. Malekhanov, A. G. Sazontov, and N. K. Vdovicheva, "Large-array gain limitations in a random oceanic waveguide with application to the North Pacific," in *Proc. 3rd Eur. Conf. on Underwater Acoustics*, Heraklion, Greece, 1996, vol. 1, pp. 507–512.

[14] N. K. Vdovicheva, E. Yu. Gorodetskaya, A. I. Malekhanov, and A. G. Sazontov, "Gain of a vertical antenna array in a randomly inhomogeneous oceanic waveguide," *Acoust. Phys.*, vol. 43, no. 6, pp. 669–675, 1997.

[15] C. C. Macaskii and B. J. Uskinski, "Propagation in waveguides containing random irregularities: The second moment equation," in *Proc. Royal Soc. London*, 1981, vol. A 377, pp. 73–98.

[16] M. J. Beran, A. M. Whitman, and S. Frankenthal, "Scattering calculations using the characteristic rays of the coherence function," *J. Acoust. Soc. Amer.*, vol. 71, no. 5, pp. 1124–1130, 1982.

[17] F. G. Bass and I. M. Fuks, *Wave Scattering from Statistically Rough Surface*. Oxford, U.K.: Pergamon, 1979.

[18] B. M. Kudryashov, "On the evaluation of acoustic fields in waveguides with statistically rough surface," in *Mathematical Problems of Geophysics*, Nauka, Novosibirsk, vol. 4, pp. 256–272, 1973 (in Russian).

[19] F. I. Kryazhev, B. M. Kudryashov, and N. A. Petrov, "Propagation of low-frequency sound waves in a waveguide with irregular boundaries," *Sov. Phys. Acoust.*, vol. 22, no. 3, pp. 21–24, 1976.

[20] W. E. Kohler and G. C. Papanicolaou, "Wave propagation in a random-inhomogeneous ocean," in *Wave Propagation and Underwater Acoustics*, vol. 70, *Lecture Notes in Physics*, J. B. Keller and J. S. Papadakis, Eds. Berlin, Germany: Springer-Verlag, 1977, pp. 153–223.

[21] L. B. Dozier and F. D. Tappert, "Statistics of normal mode amplitudes in a random ocean," *J. Acoust. Soc. Amer.*, vol. 64, no. 1, pp. 533–547, 1978.

[22] A. Beilis and F. D. Tappert, "Coupled mode analysis of multiply rough surface scattering," *J. Acoust. Soc. Amer.*, vol. 66, no. 3, pp. 811–826, 1979.

[23] G. R. Sutton and J. J. McCoy, "Spatial coherence of acoustic signals in randomly inhomogeneous waveguides—A multiple-scatter theory," *J. Math. Phys.*, vol. 18, pp. 1052–1057, 1977.

[24] G. R. Sutton, "Application of a stochastic waveguide propagation model to ocean acoustics," *J. Math. Phys.*, vol. 22, no. 12, pp. 974–976, 1981.

[25] L. S. Dolin and A. G. Nechaev, "Mode description of the acoustic field interference structure in a waveguide with statistically rough wall," *Izv. Vuzov. Radiofizika*, vol. 24, no. 11, pp. 1337–1344, 1981 (in Russian).

[26] A. A. Moiseev, "On the evaluation of field coherence function in a randomly inhomogeneous waveguide," *Dokl. Acad. Nauk SSSR*, vol. 279, no. 6, pp. 1339–1344, 1984 (in Russian).

[27] A. G. Sazontov and V. A. Farfel, "On the calculation of low-frequency sound attenuation in the ocean due to scattering by internal waves," *Akusticheskii Z.*, vol. 32, no. 4, pp. 492–498, 1986 (in Russian).

[28] V. V. Artel'nyj, V. D. Kukushkin, and M. A. Raevskij, "On the energy and correlation characteristics of low-frequency acoustic waves in underwater sound channels," *Akusticheskii Z.*, vol. 32, no. 4, pp. 591–597, 1986 (in Russian).

[29] A. G. Nechaev, "Decay of the interference structure of the sound field in an ocean with random inhomogeneities," *Sov. Phys. Acoust.*, vol. 33, no. 3, pp. 312–314, 1987.

[30] A. L. Virovlyanskij, A. G. Kosterin, and A. N. Malakhov, "Modal fluctuations in a canonical underwater sound channel," *Akusticheskii Z.*, vol. 35, no. 2, pp. 229–236, 1989 (in Russian).

[31] M. J. Beran and S. Frankenthal, "Volume scattering in a shallow channel," *J. Acoust. Soc. Amer.*, vol. 91, no. 5, pp. 3203–3211, 1992.

[32] A. G. Sazontov, "Calculation of the two-frequency mutual coherence function and the time pulse moments in a random-inhomogeneous ocean," *Sov. Phys. Acoust.*, vol. 35, no. 5, pp. 526–532, 1989.

[33] L. D. Landau and E. M. Lifshits, "Quantum mechanics," in *Theoretical Physics*. Moscow, Russia: Nauka, 1989, vol. III (in Russian).

[34] A. B. Migdal, *Qualitative Methods in Quantum Theory*. Moscow, Russia: Nauka, 1975 (in Russian).

[35] C. Garrett and W. H. Munk, "Space-time scales of internal waves: A progress report," *J. Geophys. Res.*, vol. 80, no. 3, pp. 291–297, 1975.

[36] R. Esswein and S. M. Flatte, "Calculation of the phase-structure function density from oceanic internal waves," *J. Acoust. Soc. Amer.*, vol. 70, no. 5, pp. 1387–1396, 1981.

[37] A. G. Sazontov and V. A. Farfel', "Calculation of the coherence degree and form of a pulse sound signal in an oceanic waveguide with a rough surface," *Acoust. Phys.*, vol. 41, no. 1, pp. 109–113, 1995.

[38] Ya. D. Shirman and V. N. Manzhos, *Theory and Techniques of Signal Processing in Radar*, Radio i Svyaz', Moscow, 1981 (in Russian).

[39] R. A. Monzingo and T. W. Miller, *Introduction to Adaptive Arrays*. New York: Wiley, 1980.

[40] H. P. Bucker, "Use of calculated sound fields and matched-field detection to locate sound in shallow water," *J. Acoust. Soc. Amer.*, vol. 59, no. 1, pp. 368–373, 1976.

[41] A. Tolstoy, *Matched Field Processing for Underwater Acoustics*. Singapore: World Scientific, 1993.

[42] N. V. Zuikova and V. D. Svet, "Matched-field processing of signals in ocean waveguides (review)," *Acoust. Phys.*, vol. 39, no. 3, pp. 203–210, 1993.

[43] V. I. Il'ichev, A. Ya. Kalyuzhnyi, L. G. Krasnyi, and V. Yu. Lapii, *Statistical Theory of Hydroacoustic Signal Detection*. Moscow, Russia: Nauka, 1992 (in Russian).

[44] Ya. S. Shifrin, *Problems of Statistical Array Theory*. Moscow, Russia: Sovetskoje Radio, 1970 (in Russian).

[45] B. J. Uscinski and D. E. Reeve, "The effect of ocean inhomogeneities on array output," *J. Acoust. Soc. Amer.*, vol. 87, no. 6, pp. 2527–2534, 1990.

[46] A. G. Sazontov and V. A. Farfel', "Operation of a horizontal discrete array in a randomly inhomogeneous ocean," *Sov. Phys. Acoust.*, vol. 36, no. 1, pp. 71–74, 1990.

[47] E. Yu. Gorodetskaya, A. I. Malekhanov, and V. I. Talanov, "Modeling of the optimal array signal processing in underwater sound channels," *Sov. Phys. Acoust.*, vol. 38, no. 6, pp. 571–575, 1992.

[48] E. Yu. Gorodetskaya and A. I. Malekhanov, "The theoretical gain limitations of array signal processing in underwater sound channels," in *Proc. 2nd Europ. Conf. on Underwater Acoustics*, Luxemburg, Germany, 1994, pp. 665–670.

[49] C. H. Knapp, "Signal detectors for deformable hydrophone arrays," *IEEE Trans. Acoust., Speech, Signal Processing*, vol. 37, pp. 1–7, Jan. 1989.

[50] A. I. Malekhanov and V. I. Talanov, "Optimal signal reception in multimode waveguides," *Sov. Phys. Acoust.*, vol. 36, no. 5, pp. 496–499, 1990.

[51] W. J. Pierson and L. Moskowitz, "A proposed spectral form for fully developed wind seas based on the similarity theory of S. A. Kitaigorodskii," *J. Geophys. Res.*, vol. 69, no. 24, pp. 5181–5190, 1964.

[52] W. A. Kuperman and F. Ingenito, "Spatial correlation of surface generated noise in a stratified ocean," *J. Acoust. Soc. Amer.*, vol. 67, no. 6, pp. 1988–1996, 1980.

[53] A. I. Malekhanov, "Incoherent spatial mode filtering in randomly inhomogeneous ocean waveguides," *Sov. Phys. Acoust.*, vol. 38, no. 5, pp. 489–493, 1992.

[54] S. M. Flatte and R. B. Stoughton, "Predictions of internal-wave effects on ocean acoustic coherence, travel-time variance, and intensity moments for very long-range propagation," *J. Acoust. Soc. Amer.*, vol. 84, no. 4, pp. 1414–1424, 1988.

[55] T. Stefanick, *Strategic Antisubmarine Warfare and Naval Strategy*. Toronto, Canada: Lexington, 1987.

Elena Yu. Gorodetskaya was born in Nizhny Novgorod (formerly Gorky), Russia, in 1967. She received the M.S. degree in computational mathematics from the Gorky State University in 1989.

Since 1989, she has been with the Division of Hydrophysics and Hydroacoustics of the Institute of Applied Physics, Russian Academy of Science, Nizhny Novgorod, and is presently a Junior Research Scientist. Her research interests include computer simulations in the field of array signal processing.

Ms. Gorodetskaya received the Distinguished Young Scientist Governmental Fellowship in 1997–1999.

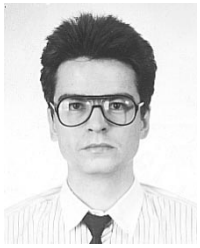

Alexander I. Malekhanov was born in Nizhny Novgorod (formerly Gorky), Russia, in 1960. He received the M.S. degree in physics from the Moscow Engineering Physics Institute in 1983 and the candidate of science degree (analogous to the Ph.D. degree) in radio physics from the Nizhny Novgorod State University in 1998.

Since 1983, he has been with the Division of Hydrophysics and Hydroacoustics of the Institute of Applied Physics, Russian Academy of Science, Nizhny Novgorod, and is presently a Senior Research Scientist. Since 1993, he has also been a Lecturer at the Department of Radio Physics of the Nizhny Novgorod State University. His research interests include antenna theory and signal processing with applications to underwater acoustics.

Dr. Malekhanov received the URSI Young Scientist Award at the 24th URSI General Assembly (1993). He is a member of the Russian Acoustical Society.

Alexander G. Sazontov was born in Nizhny Novgorod (formerly Gorky), Russia, in 1952. He received the M.S. degree in physics from the Gorky State University in 1975 and the Ph.D. degree in geophysics from the Institute of Applied Physics, Russian Academy of Science in 1982.

He worked at the Radio Physical Research Institute, Gorky (1975–1977), where he performed research on statistical theory of strong and weak turbulence in a stratified ocean. Since 1982, he has been a Senior Research Scientist in the Division of Hydrophysics and Hydroacoustics of the Institute of Applied Physics, Russian Academy of Science, Nizhny Novgorod. In 1998, he became head of the Laboratory of Statistical Methods in Ocean Acoustics. His research interests are in physical oceanography, wave propagation and scattering in random media, and spatial-temporal signal processing. Since 1984, most of his research has been in underwater acoustic coherence at long ranges and its applications.

Nadezhda K. Vdovicheva was born in Nizhny Novgorod (formerly Gorky), Russia, in 1954. She received the M.S. degree in mathematics from the Gorky State University in 1976 and the Ph.D. degree in mathematical simulation of physical processes from the Institute of Applied Physics, Russian Academy of Science in 1990.

She worked at the Institute of Applied Physics, Gorky (1976–1993), where she performed research on mathematical simulation of sound propagation in a stratified ocean. Since 1993, she has been a Research Scientist at the Institute for Physics of Microstructures, Russian Academy of Science, Nizhny Novgorod. Her research interests include wave propagation, mathematical simulation in underwater acoustics, computational mathematics, and software design.